Monthly Notices of the ROYAL ASTRONOMICAL SOCIETY

MNRAS **527,** 8907–8920 (2024) https://doi.org/10.1093/mnras/stad3803
Advance Access publication 2023 December 11

Orbits and dynamical masses for the active Hyades multiple system HD 284163

Guillermo Torres [1]★ Gail H. Schaefer [2] Robert P. Stefanik,[1] David W. Latham [1] Jeremy Jones [2] Cyprien Lanthermann [2] John D. Monnier [3] Stefan Kraus [4] Narsireddy Anugu [2] Theo ten Brummelaar [2] Sorabh Chhabra,[4] Isabelle Codron [4] Jacob Ennis [3] Tyler Gardner [4] Mayra Gutierrez,[3] Noura Ibrahim [3] Aaron Labdon [5] Dan Mortimer [4] and Benjamin R. Setterholm [3]

[1]*Center for Astrophysics|Harvard & Smithsonian, 60 Garden St, Cambridge, MA 02138, USA*
[2]*The CHARA Array of Georgia State University, Mount Wilson Observatory, Mount Wilson, CA 91203, USA*
[3]*Astronomy Department, University of Michigan, Ann Arbor, MI 48109, USA*
[4]*Astrophysics Group, Department of Physics & Astronomy, University of Exeter, Stocker Road, Exeter EX4 4QL, UK*
[5]*European Southern Observatory, Casilla 19001, Santiago 19, Chile*

Accepted 2023 November 20. Received 2023 October 20; in original form 2023 September 1

ABSTRACT

We report near-infrared long-baseline interferometric observations of the Hyades multiple system HD 284163, made with the Center for High Angular Resolution Astronomy array, as well as almost 43 yr of high-resolution spectroscopic monitoring at the Center for Astrophysics. Both types of observations resolve the 2.39 d inner binary, and also an outer companion in a 43.1 yr orbit. Our observations, combined with others from the literature, allow us to solve for the 3D inner and outer orbits, which are found to be at nearly right angles to each other. We determine the dynamical masses of the three stars (good to better than 1.4 per cent for the inner pair), as well as the orbital parallax. The secondary component (0.5245 ± 0.0047 $M_{\odot}$) is now the lowest mass star with a dynamical mass measurement in the cluster. A comparison of these measurements with current stellar evolution models for the age and metallicity of the Hyades shows good agreement. All three stars display significant levels of chromospheric activity, consistent with the classification of HD 284163 as an RS CVn object. We present evidence that a more distant fourth star is physically associated, making this a hierarchical quadruple system.

Key words: astrometry – binaries: close – binaries: spectroscopic – stars: fundamental parameters – stars: individual: HD 284163 – techniques: spectroscopic.

1 INTRODUCTION

The Hyades cluster has a long history of astrometric, photometric, and spectroscopic observations dating back more than a century. At a mean distance of only ∼45 pc, this collection of roughly 800 members (e.g. Brandner, Calissendorff & Kopytova 2023), all of the same age and chemical composition (∼750 Myr, [Fe/H] = +0.18; Brandt & Huang 2015; Dutra-Ferreira et al. 2016), has served as a valuable laboratory for astrophysics. It is also rich in binary and multiple systems (see e.g. Griffin et al. 1985, 1988; Griffin 2012, and references therein), and yet relatively few of them have had their most basic property – their masses – determined dynamically. For the most recent determinations and a summary of earlier estimates, we refer the reader to the work by Torres, Stefanik & Latham (2019) and Brogaard et al. (2021). Knowledge of the mass constrains models of stellar evolution in ways that complement the information that can be obtained perhaps more easily, such as luminosities and temperatures, and permits valuable tests of theory. When in a cluster of known age and composition, such as the Hyades, the constraint is strengthened because there are then fewer free parameters that one can adjust in the models in order to match the observations. This is especially interesting for compositions significantly different from solar, as is the case for the Hyades.

Not all available mass measurements in the Hyades reach precisions at the level of 1–3 per cent, which are most useful for a comparison with stellar models (see e.g. Torres, Andersen & Giménez 2010). Some are considerably worse, with errors up to 15 per cent. Furthermore, only well detached binaries with no prior history of mass exchange are suitable for such tests. We count seven suitable systems to date, excluding the case of V471 Tau, which is a post-common envelope eclipsing binary composed of a K dwarf and a DA white dwarf (Muirhead, Nordhaus & Drout 2022). That system is not representative of single-star evolution because of the past interaction of the components.

This paper reports precise mass measurements for another system in the Hyades, HD 284163 (BD + 23 635, Pels 20, V1136 Tau; $V = 9.41$), as part of an ongoing programme designed to significantly enlarge the sample of such determinations in the cluster. HD 284163 is classified as a K0 dwarf, and was first recognized as a Hyades

★ E-mail: gtorres@cfa.harvard.edu

member by Luyten (1971) and Pels, Oort & Pels-Kluyver (1975). It has long been thought to be a binary from its location well above the single-star main sequence of the Hyades (Upgren & Weis 1977). It was found to be a single-lined spectroscopic binary by Griffin & Gunn (1981), who established the period to be 2.39 d. However, despite the ∼0.8 mag excess in brightness compared to a single star of the same colour, those authors found only subtle and indirect evidence of a companion from slight distortions in the radial velocities obtained near conjunction. This was somewhat surprising, as a companion raising the total brightness by as much as 0.8 mag should be rather obvious. A note added in proof to the Griffin & Gunn (1981) paper finally showed this companion more clearly in a pair of spectra obtained later, but pointed out the unexpected fact that its velocity was stationary, indicating it is not the secondary in the 2.39 d orbit. They then remarked that the object '...might well repay careful examination, either directly or by interferometric or occultation studies, for visual duplicity'. This suspicion proved correct, and a few years later speckle interferometric observations by McAlister et al. (1987) revealed a visual companion at a separation of about 0.14 arcsec, which we now identify with the stationary signal found by Griffin & Gunn (1981). Subsequent speckle measurements by others showed this wide companion to be in a ∼40 yr orbit around the inner pair (Mason & Hartkopf 2010), making the HD 284163 system a hierarchical triple. Third components in close spectroscopic binaries are not unexpected, as Tokovinin et al. (2006) have shown that more than 95 per cent of systems with periods under 3 d are attended by a more distant companion. The elusive secondary of the 2.39 d binary, an M dwarf several magnitudes fainter than the primary, was finally detected in near infrared observations by Bender & Simon (2008).[1]

HD 284163 was placed on our target list for long-baseline interferometric observations with the Center for High Angular Resolution Astronomy (CHARA) Array (ten Brummelaar et al. 2016), with the goal of resolving the inner pair to determine the component masses. As we describe here, those observations were successful despite the small, ∼1 mas semimajor axis of the orbit. The tertiary was resolved as well. HD 284163 has also been monitored spectroscopically for more than 40 yr, as part of a large survey of several hundred stars in the Hyades region carried out at the Center for Astrophysics (CfA). These high-resolution spectroscopic observations have clearly revealed the lines of the faint secondary, allowing us to measure its radial velocity with higher precision than before. All of this material combined has enabled us to obtain highly precise measurements of the masses for the inner pair, as well as the brightness of each component, and the orbital parallax. We also take the opportunity to update the astrometric orbit of the wide pair, which is necessary in order to avoid biasing the mass determinations. Hierarchical triples such as this, in which the full 3D inner and outer orbits can be determined, as we show below, are particularly useful to study the architectures of these systems. They can provide insight into effects such as the Lidov–Kozai cycles, which have the ability to shape their long-term evolution (see, e.g. Toonen, Hamers & Portegies Zwart 2016).

[1]Bopp, Africano & Goodrich (1986) may have detected it earlier. One of their spectra from 1982 showed a strongly redshifted Hα line in emission, very near the velocity we now expect for the secondary, along with absorption lines at about the right velocity for the other two components. However, they dismissed this possibility because of anomalous behaviour of the Hα line in an earlier photographic spectrum, which had the lines of the two main components blended.

Table 1. Interferometric calibrator stars.

Star	UD_H (mas)	UD_K (mas)	σ_{UD} (mas)
HD 17660	0.3053	0.3069	0.0073
HD 20150	0.3499	0.3506	0.0127
HD 23288	0.2277	0.2282	0.0068
HD 24702	0.2441	0.2450	0.0057
HD 27627	0.2727	0.2740	0.0062
HD 27808	0.2748	0.2758	0.0066
HD 28406	0.2766	0.2775	0.0069
HD 36667	0.2839	0.2849	0.0069

Note. Uniform disc diameters in the *H* and *K* bands adopted from the JMMC Stellar Diameter Catalogue (Bourges et al. 2017).

Our interferometric and spectroscopic observations are reported in Section 2, along with previously obtained measurements of the relative position of the tertiary, made mostly with the speckle technique. Our own measurements of the third star are given there as well. The orbital analysis to derive the inner and outer orbits simultaneously is described in Section 3. In Section 4, we compile evidence for a fourth star in the system, and Section 5 reports on the many signs of activity in HD 284163. Stellar evolution models are then used in Section 6 for a comparison against the observations. Our final thoughts are given in Section 7.

2 OBSERVATIONS

2.1 Interferometry with CHARA

The CHARA Array is located at Mount Wilson Observatory, and combines the light of six 1m telescopes with baselines ranging from 34 to 331 m (ten Brummelaar et al. 2005). Each telescope is equipped with an adaptive optics system that improves the sensitivity for fainter targets such as HD 284163 (Che et al. 2013; Anugu et al. 2020). We observed the object on five nights using the Michigan InfraRed Combiner-eXeter (MIRC-X) *H*-band combiner in the low-resolution Prism50 mode (Anugu et al. 2020). On the last two nights we observed simultaneously with the Michigan Young STar Imager at CHARA (MYSTIC) *K*-band combiner in Prism49 mode (Setterholm et al. 2023). MIRC-X and MYSTIC combine the light from all six telescopes (S1, S2, E1, E2, W1, and W2), providing spectrally dispersed visibilities on 15 baselines and closure phases on 20 triangles. To calibrate the interferometric transfer function, we alternated between observations of unresolved calibrator stars and the science targets. The calibrators were selected using SearchCal.[2] The adopted uniform disc diameters for the calibrators in the *H* and *K* bands (UD_H and UD_K) are listed in Table 1.

The MIRC-X and MYSTIC data were reduced using the standard pipeline (version 1.3.5) written in python.[3] On each night the calibrators were calibrated against each other; no evidence of binarity was found in the calibrators based on visual inspection. The calibrated OIFITS files for HD 284163 will be available in the Optical Interferometry Database[4] and the CHARA Data Archive.[5]

The interferometric field of view is set by the coherence length of the beam combiner ($\lambda^2/\Delta\lambda$). For the low-resolution ($R = 50$) spectral

[2]https://jmmc.fr/searchcal
[3]https://gitlab.chara.gsu.edu/lebouquj/mircx_pipeline.git
[4]http://jmmc.fr/~webmaster/jmmc-html/oidb.htm
[5]https://www.chara.gsu.edu/observers/database

Table 2. CHARA measurements for the inner binary of HD 284163.

UT Date	HJD (2400000+)	τ (d)	ρ (mas)	θ (deg)	σ_{maj} (mas)	σ_{min} (mas)	θ_σ (deg)	f_{Ab}/f_{Aa}	f_B/f_{Aa}	Instrument
2020 Oct 22	59144.812	−0.0470	0.8635	46.39	0.0093	0.0061	132.79	0.2181	0.7073	MIRC-X (*H* band)
2020 Oct 23	59145.862	−0.0470	0.6800	214.46	0.0033	0.0024	123.84	0.2540	0.5623	MIRC-X (*H* band)
2020 Nov 12	59165.853	−0.0470	0.4241	273.60	0.0085	0.0054	123.45	0.2817	0.5184	MIRC-X (*H* band)
2020 Nov 12	59165.931	−0.0470	0.3957	308.54	0.0455	0.0306	129.60	0.1396	0.4697	MIRC-X (*H* band)
2021 Nov 19	59537.847	−0.0461	0.8857	65.72	0.0051	0.0047	164.38	0.2304	0.3601	MIRC-X (*H* band)
2021 Nov 19	59537.847	−0.0461	0.8871	65.91	0.0093	0.0073	67.18	0.2577	0.5138	MYSTIC (*K* band)

Note. Column τ gives the light traveltime corrections to be added to the dates of observation, to refer them to the centre of mass of the triple system. All angles are on the ICRS (effectively J2000). Formal uncertainties for the flux ratios f_{Ab}/f_{Aa} and f_B/f_{Aa} are not reported, as they are typically unrealistically small. A more representative value for the flux uncertainties is given by the scatter of the measurements (see Section 6).

mode of MIRC-X, this translates to 0.05 arcsec on the longest 331 m baseline and 0.5 arcsec on the shortest 34 m baseline. Therefore, the wide tertiary companion is within the interferometric view of the shortest baselines (produces visibility modulation), but it is resolved out on the longer baselines (incoherent light produces a constant scaling factor). We followed a two step approach for modelling the CHARA data. First, we removed the data on the shorter baselines that are most impacted by the wide companion ($B < 110$ m for most dates, and $B < 70$ m for UT 2021 November 19), and fit a simple binary model to the data. We used the Interactive Data Language (IDL) adaptive grid search procedure[6] (Schaefer, Hummel & Gies 2016) to solve for the separation (ρ), position angle east of north (θ) on the International Celestial Reference System (ICRS), and the fractional fluxes of two inner components (f_{Aa}, f_{Ab}). We added a scaling factor (f_B) to account for incoherent flux from the outer component in the field of view. The CHARA measurements for the inner pair of HD 284163 (Ab relative to Aa) are reported in Table 2, together with the flux contribution of the third star, expressed as the ratio f_B/f_{Aa}.

We then fit the CHARA data on all baselines using the triple model described by Schaefer, Hummel & Gies (2016) that includes band-width smearing. The triple model accounts for the fast visibility modulations on the shortest baselines from the wide tertiary companion. As a starting position for the triple fit, we used our measurements of the inner pair (Table 2) and estimated the position of the outer component based on an orbit fit to the speckle observations described in Section 2.3. We then performed a grid search where we varied the position of the outer pair over a range of ±20 mas in 0.5 mas steps. At each position in the grid, we optimized the separations and flux ratios of the inner and outer pairs by performing a Levenberg–Marquardt least-squares minimization using the IDL MPFIT[7] routine (Markwardt 2009). The CHARA measurements of the position of HD 284163 B relative to Aa are reported in Table 3. For the two sets of data collected on UT 2020 November 12, we did not have the E2 telescope in the first set and lost delay on the E1 telescope in the second set. Therefore, we fit the triple based on the combined data for the two sets collected that night to improve the *uv* coverage on the sky. In all cases, the triple solution produced positions for the close pair that are consistent with the simpler binary fit.

The apparent sizes of the stars are unresolved by our observations, even at the longest baselines. Consequently, for the binary and triple fits, we adopted fixed stellar angular diameters of 0.171, 0.125, and 0.143 mas, respectively for components Aa, Ab, and B. These were estimated from preliminary masses for the components and radii as predicted by stellar evolution models described later. The precise values of the diameters have a negligible effect on the results. During the fitting process, we also divided the wavelengths in the OIFITS files by systematic correction factors of 1.0054 ± 0.0006 for MIRC-X and 1.0067 ± 0.0007 for MYSTIC (J. D. Monnier, priv. comm.). On UT 2022 November 15, the S1 and S2 telescopes were offline because of technical problems. The resulting *uv* coverage provided by the E1, E2, W1, and W2 telescopes covered only a narrow swath on the sky and was insufficient for modelling the triple system.

[6] https://www.chara.gsu.edu/analysis-software/binary-grid-search
[7] http://cow.physics.wisc.edu/~craigm/idl/idl.html

2.2 Spectroscopic observations

Our spectroscopic observations of HD 284163 at the CfA began on New Years day, 1980. They were gathered with three different instruments on two telescopes, as we now describe.

Observations through 2006 December were made with two nearly identical echelle instruments on the 1.5m Wyeth reflector at the (now closed) Oak Ridge Observatory (Massachusetts, USA), and on the 1.5m Tillinghast reflector at the Fred L. Whipple Observatory (Arizona, USA). These instruments (Digital Speedometers; Latham 1992) delivered a resolving power of $R \approx 35\,000$, and used intensified photon-counting Reticon detectors that recorded a single order 45 Å wide centred at a wavelength of 5187 Å. The main spectral features in this region are the lines of the Mg I b triplet. We obtained a total of 88 spectra with these instruments. Those collected through the end of the 2003 observing season have signal-to-noise ratios between 10 and 22 per resolution element of 8.5 km s^{-1}. Beginning in 2004, exposures were lengthened to look for signs of the secondary, reaching signal-to-noise ratios of 36–60. Wavelength solutions for these observations relied on exposures of a thorium–argon lamp taken before and after each science exposure. The zero point of the velocity system was monitored with observations of the sky at dusk and dawn. Small run-to-run corrections based on them were applied as described by Latham (1992), to place observations from both instruments on the same native CfA system. This system is slightly offset from the IAU system by 0.14 km s^{-1} (Stefanik, Latham & Torres 1999), as determined from observations of minor planets in the solar system. We removed this shift by adding +0.14 km s^{-1} to all our raw velocities from the Digital Speedometers.

From 2011 January until 2022 December, we continued the observations with the Tillinghast Reflector Echelle Spectrograph (TRES; Szentgyorgyi & Fűrész 2007; Fűrész 2008) on the 1.5m telescope in Arizona. This bench-mounted, fibre-fed instrument delivers a resolving power of $R \approx 44\,000$, and has a CCD detector that records 51 echelle orders between 3800 and 9100 Å. We collected 20

Table 3. CHARA measurements for the tertiary of HD 284163.

UT Date	HJD (2400000+)	ρ (mas)	θ (deg)	σ_{maj} (mas)	σ_{min} (mas)	θ_σ (deg)	Instrument
2020 Oct 22	59144.812	184.888	220.290	0.112	0.074	14.121	MIRC-X (*H* band)
2020 Oct 23	59145.862	186.287	220.147	0.094	0.071	31.168	MIRC-X (*H* band)
2020 Nov 12	59165.893	184.288	220.641	0.071	0.025	41.062	MIRC-X (*H* band)
2021 Nov 19	59537.847	175.733	224.485	0.118	0.028	47.808	MIRC-X (*H* band)
2021 Nov 19	59537.847	175.675	224.460	0.108	0.029	47.516	MYSTIC (*K* band)

Note. The CHARA measurements of the tertiary of HD 284163 (star B) are made relative to the primary (star Aa). The meaning of the columns is similar to Table 2.

spectra with signal-to-noise ratios of 41–110 per resolution element of 6.8 km s^{-1}. During each run we used observations of IAU standard stars to monitor changes in the velocity zero-point of TRES, and observations of asteroids to translate the raw velocities to an absolute system, as done with the Digital Speedometers.

The weaker exposures from the Digital Speedometers, through the end of 2003, show only the lines of the primary of the inner pair (hereafter star Aa) and of the tertiary (star B). The stronger Digital Speedometer exposures obtained later also reveal the much fainter lines of star Ab, the secondary in the inner binary. All of the TRES observations show the lines of the three stars.

Radial velocities (RVs) for the double-lined spectra were measured using TODCOR (Zucker & Mazeh 1994), a two-dimensional cross-correlation technique. Those in which the three stars are visible were measured with TRICOR (Zucker, Torres & Mazeh 1995), which is an extension of TODCOR to three dimensions. The templates were taken from a pre-computed library of calculated spectra based on model atmospheres by R. L. Kurucz, and a line list tuned to better match real stars (see Nordström et al. 1994; Latham et al. 2002). The microturbulent velocity in these models was set to 2 km s^{-1}, and the macroturbulent velocity to 1 km s^{-1}. For the TRES instrument, we used only the order centred on the Mg 1 b triplet, so as to match the spectral region of the Digital Speedometers. Experience has shown that this is also the order that provides most of the velocity information.

The optimal template parameters were determined by running grids of cross-correlations on the higher-quality TRES spectra, as described by Torres, Neuhäuser & Guenther (2002), and choosing the values in our grid nearest to those best fits. The effective temperatures adopted for the templates are $T_{\rm eff} = 5000$ and 4500 K for stars Aa and B, respectively. Star Ab is too faint for us to determine its template parameters in the same way. The temperature in this case was taken to be 3750 K, consistent with the properties of that star determined later. Surface gravities of $\log g = 4.5$ were held fixed for all three stars, along with solar composition, which is sufficiently close to the metallicity of the Hyades for our purposes ([Fe/H] = +0.18 ± 0.03; Dutra-Ferreira et al. 2016). For the primary template, we used a rotational broadening $V_{\rm rot}$ of 20 km s^{-1}, which includes macroturbulence, and for stars Ab and B we found non-rotating templates to provide the highest cross-correlation values ($V_{\rm rot}$ values significantly below the TRES resolution of 6.8 km s^{-1} are uncertain). Estimates of the temperatures and $V_{\rm rot}$ for Aa and B to a finer resolution than the sampling of our template library were made by interpolation, resulting in values of $T_{\rm eff} = 4990 \pm 100$ K and 4510 ± 200 K, with rotational velocities of $V_{\rm rot} = 18.4 \pm 1.0$ km s^{-1} and $V_{\rm rot} < 2$ km s^{-1}, respectively. An independent estimate of the rotation of the primary by Mermilliod, Mayor & Udry (2009) gave 19.3 ± 2.0 km s^{-1}, in good agreement with ours. We list our velocities in Table 4, along with their formal uncertainties.

We also used our spectra to determine the relative brightness of the components. From the Digital Speedometer observations we obtained light ratios of $f_{\rm Ab}/f_{\rm Aa} = 0.028 \pm 0.012$ and $f_{\rm B}/f_{\rm Aa} = 0.110 \pm 0.010$ in the Mg 1 b order. The TRES observations resulted in similar ratios of $f_{\rm Ab}/f_{\rm Aa} = 0.028 \pm 0.004$ and $f_{\rm B}/f_{\rm Aa} = 0.130 \pm 0.006$. We adopt weighted averages of $f_{\rm Ab}/f_{\rm Aa} = 0.028 \pm 0.004$ and $f_{\rm B}/f_{\rm Aa} = 0.125 \pm 0.010$. These are all considerably lower than the near infrared values reported above, because the secondary and tertiary are less massive than the primary, so their flux contribution in the optical is smaller.

Aside from our own RVs, the only other significant set of measurements is that of Griffin & Gunn (1981), which are the earliest for HD 284163 (1974–1980), and can help to constrain the outer orbit. We therefore included these 41 RVs of star Aa in the analysis of Section 3, with the weights assigned by the authors to the individual observations.

Two other short sets of measurements are available in the literature. Mermilliod, Mayor & Udry (2009) published four RVs made with the CORAVEL spectrometer at the Haute-Provence Observatory (France), which have similar precision as those of Griffin & Gunn (1981), and were obtained at similar epochs (1978–1984). Although the publication does not identify which component they refer to, one of the measurements, on HJD 2445376.347, happens to be of star B, and the other three are of star Aa. We have incorporated these observations into our analysis as well. Another set of five RV measurements of HD 284163 was obtained in 2004–2005 by Bender & Simon (2008), who observed in the near infrared to facilitate the detection of the faint star Ab. While they succeeded (and only reported the velocities for that star), the measurements have relatively large uncertainties and are not as useful for our analysis.

2.3 Speckle observations

HD 284163 has been followed more or less regularly by speckle observers since the discovery of its 0.″14 outer companion in 1985. Some two dozen measurements of the position of star B relative to the inner binary have been reported to date. A listing of these measurements from the Washington Double Star Catalog (WDS; Worley & Douglass 1997; Mason et al. 2001) was kindly provided by R. Matson (USNO). The double star designation and discoverer name in the catalogue are, respectively, WDS J04119+2338A and CHR 14. Two adaptive optics measurements by Morzinski (2011) and one from Asensio-Torres et al. (2018) were added by us to this list, and a few minor adjustments to other WDS entries were made after consulting the original sources. Additional measurements from our own observations with CHARA have been given earlier in Table 3, and are typically about an order of magnitude more precise than the speckle measurements. Fig. 1 is a graphical representation

Table 4. CfA radial velocity measurements for HD 284163.

HJD (2400000+)	τ (d)	Year	RV_{Aa} (km s^{-1})	RV_{Ab} (km s^{-1})	RV_{B} (km s^{-1})	Inner phase	Outer phase	Instrument
44239.6115	−0.0448	1979.9988	58.61 ± 1.01	...	...	0.9920	0.6948	1
44600.7619	−0.0435	1980.9876	− 10.32 ± 0.92	...	41.19 ± 1.85	0.8259	0.7177	1
44603.6784	−0.0435	1980.9956	81.32 ± 1.63	...	37.46 ± 3.27	0.0440	0.7179	1
44627.6345	−0.0434	1981.0612	83.39 ± 1.75	...	35.22 ± 3.51	0.0492	0.7194	1
44629.6401	−0.0434	1981.0667	13.07 ± 0.95	...	40.77 ± 1.91	0.8869	0.7196	1

Note. Column τ is the light traveltime correction in the outer orbit, applied in the analysis of Section 3 to refer the ephemerides to the barycentre of the triple system. The formal RV uncertainties listed here are adjusted iteratively in the orbital analysis described later. Phases in the inner and outer orbits were computed from the ephemerides given in Section 3. The instrument code in the last column is 1 for the Digital Speedometers and 2 for TRES. (This table is available in its entirety in machine-readable form).

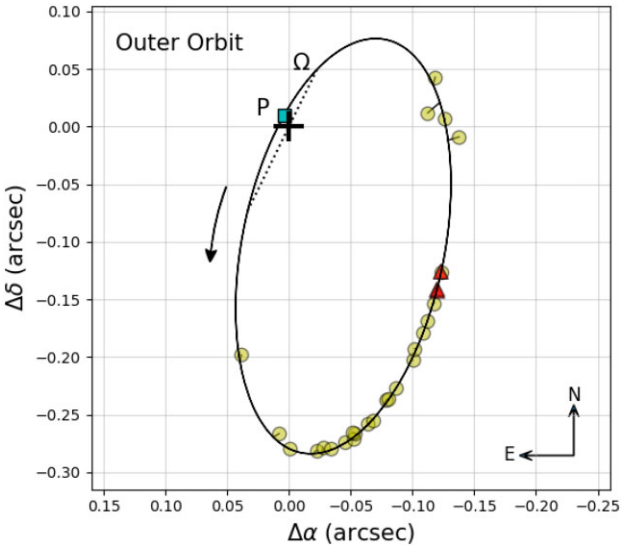

Figure 1. Measured relative positions of the tertiary in HD 284163, together with our best-fitting model described in Section 3. The '+' symbol represents the centre of light of the inner binary, which is unresolved in the speckle observations. Short line segments connect the observed positions with the predicted location in the orbit. Circles represent observations from the WDS, and red triangles are our own measurements from CHARA. The square labelled 'P' represents periastron, and the line of nodes is indicated with a dotted line, where 'Ω' marks the ascending node.

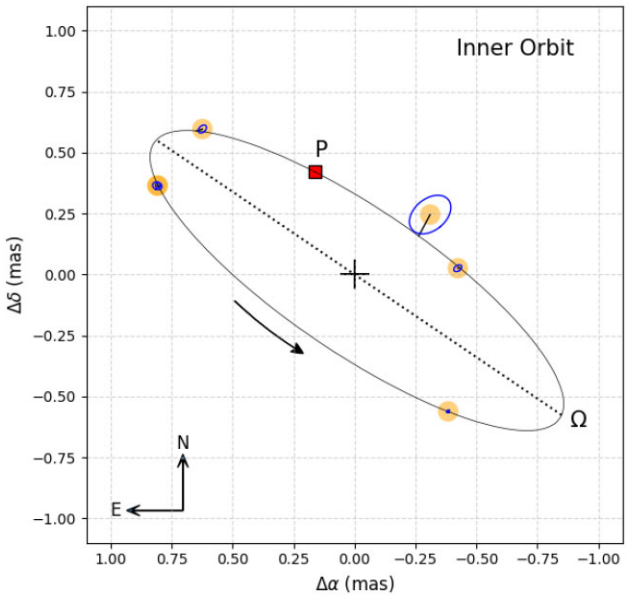

Figure 2. CHARA observations of the inner binary in HD 284163 (highlighted with orange circles) with their corresponding error ellipses, along with our model for the astrometric orbit described later. The '+' sign represents the primary (star Aa). Short line segments connect the observed positions with the predicted location in the orbit. The dotted line represents the line of nodes (ascending node labelled 'Ω'), and the square labelled 'P' marks the location of periastron.

of these observations, along with our best-fitting model described below.

3 ANALYSIS

An initial spectroscopic solution for the orbit of stars Aa and Ab around each other displayed an obvious pattern in the RV residuals with time, reflecting a drift in the centre-of-mass velocity due to the motion of the inner pair in the ∼40 yr outer orbit. To properly account for this drift, the approach we have taken here is to solve for the elements of the inner and outer orbits simultaneously, using all observations together. The radial velocities cover an interval of 48 yr, and the speckle observations span 36 yr. We assume here that the motions in the inner and outer orbits are unperturbed by tidal interactions, i.e. that they are purely Keplerian. This is justified given the large period ratio of roughly 1:6600 (see below).

The inner astrometric orbit, as mapped by the CHARA observations, is described by the period (P_A), the angular semimajor axis (a''_A), the eccentricity and argument of periastron for the secondary (via the parameters $\sqrt{e_A}\cos\omega_{Ab}$ and $\sqrt{e_A}\sin\omega_{Ab}$), the cosine of the orbital inclination angle ($\cos i_A$), the position angle of the ascending node for the equinox of 2000.0 (Ω_A), and a reference time of periastron passage ($T_{peri,A}$). Similar elements are used to represent the outer orbit, indicated with the subindex 'AB'. The corresponding argument of periastron for the tertiary in the wide orbit is ω_B. The spectroscopic orbit of the inner binary requires two additional parameters, K_{Aa} and K_{Ab}, to represent the velocity semiamplitudes. The radial velocity motion in the outer orbit has similar parameters, K_A and K_B. The centre-of-mass velocity of the triple system is γ.

Not all of these elements are strictly necessary to describe the motion of the components. This comes from the fact that the inner orbit is covered by both spectroscopic and astrometric observations, which enables the orbital parallax to be obtained, as follows:

$$\pi_{orb} = \frac{2\pi}{P_A}\frac{a''_A \sin i_A}{\sqrt{1-e_A^2}(K_{Aa}+K_{Ab})}\,. \quad (1)$$

An analogous formula for the orbital parallax may be written using the elements of the outer orbit. Equating those two expressions, we obtain the following relation among the orbital elements:

$$K_{\rm A} + K_{\rm B} = \frac{a''_{\rm AB}}{a''_{\rm A}} \frac{\sin i_{\rm AB}}{\sin i_{\rm A}} \frac{P_{\rm A}}{P_{\rm AB}} \frac{\sqrt{1-e_{\rm A}^2}}{\sqrt{1-e_{\rm AB}^2}} (K_{\rm Aa} + K_{\rm Ab}) \,. \quad (2)$$

One of these elements is therefore redundant, and here we have chosen to eliminate $K_{\rm A}$.

In Section 2.2, we noted the somewhat arbitrary choice of the template for component Ab, due to the fact that we could not establish its parameters independently because of the faintness of the star. This has the potential to introduce systematic errors in the velocities of Ab, which could bias the mass determinations. To guard against this, we introduced two additional free parameters in our solution to represent possible offsets of the Ab velocities with respect of those of Aa, one for the Digital Speedometer observations ($\Delta_{\rm DS}$) and another for TRES ($\Delta_{\rm TRES}$). Similarly, we allowed for one more offset applied to the Griffin & Gunn (1981) velocities of star Aa ($\Delta_{\rm GG}$) to bring them onto the same reference frame as the CfA observations. The CORAVEL observations of Mermilliod, Mayor & Udry (2009) are nominally on the IAU system, as are ours, so no offset is necessary. Both Griffin & Gunn (1981) and Mermilliod, Mayor & Udry (2009) reported velocities for only one component at each epoch (usually star Aa), ignoring the presence of the others. While stars Ab and B are considerably fainter, in principle they can still introduce a subtle bias in the measurements of Aa at certain phases, which could affect its velocity semiamplitude and consequently the masses. We would expect this effect to show up in the velocity residuals, but as seen in a figure below, we do not detect such a bias at a significant level compared to the uncertainties. We therefore concluded it is safe to include these measurements of star Aa (and B, in the case of one observation from Mermilliod, Mayor & Udry 2009).

All in all we used 88, 14, and 87 Digital Speedometer RVs for stars Aa, Ab, and B, respectively, 20, 18, and 20 RVs from TRES, 41 RVs of star Aa from Griffin & Gunn (1981), and 3 of star Aa and one of star B from Mermilliod, Mayor & Udry (2009). The astrometric observations consisted of 6 pairs of (θ, ρ) observations from CHARA for the inner binary, 5 pairs of CHARA measurements of the tertiary, and 25 pairs from the WDS catalogue for the outer orbit. The CHARA measurements for the tertiary are relative to the primary star (Aa), and were corrected at each iteration in the analysis to refer them to the inner binary's centre of mass. Strictly speaking, the WDS observations of the tertiary are made relative to the centre of light of the binary, but the offset from the centre of mass is negligible given the precision of those measurements. All angles from the speckle observations have been uniformly precessed to the year 2000.0.

A joint orbital analysis of all the observations was carried out in a Markov chain Monte Carlo (MCMC) framework, using the EMCEE[8] package of Foreman-Mackey et al. (2013). The chains had 20 000 links after burn-in, and we adopted uniform priors over suitable ranges for most adjustable parameters. Convergence was checked by visual inspection of the chains, and by requiring a Gelman–Rubin statistic of 1.05 or smaller (Gelman & Rubin 1992).

Despite the best efforts by observers, it is not uncommon for measurement errors to be either too small or too large. To ensure proper weights for each data set, we allowed for additional free parameters in our analysis to represent multiplicative scale factors applied to the formal uncertainties for each kind of observation. Two such parameters were used for the position angles and separations from the WDS observations (f_θ and f_ρ), one to scale the error ellipses of the CHARA observations of the inner binary ($f_{\rm CHARA,A}$), and another for the tertiary measurements ($f_{\rm CHARA,AB}$). Three additional ones were used for the RVs of each component from the Digital Speedometers ($f_{\rm Aa,DS}$, $f_{\rm Ab,DS}$, $f_{\rm B,DS}$), another three for TRES ($f_{\rm Aa,TRES}$, $f_{\rm Ab,TRES}$, $f_{\rm B,TRES}$), and one more for the Griffin & Gunn (1981) velocities of star Aa ($f_{\rm Aa,GG}$). The Mermilliod, Mayor & Udry (2009) measurements were considered as part of the TRES data set. Lognormal priors were adopted for all of these error scaling factors. The total number of adjustable parameters in our analysis is 32.

At each iteration we adjusted the times of observation of the RVs and CHARA measurements to account for light traveltime in the wide orbit, following Irwin (1952, 1959). The times of periastron passage reported below are therefore referred to the barycentre of the triple system. The corrections τ range from -0.0482 to -0.0023 d, and are not negligible compared to the period of the inner orbit, amounting to up to 0.02 in phase. These corrections are listed in Tables 2 and 4.

The results of our MCMC analysis are presented in Table 5, where for the benefit of the reader we list the elements for the inner and outer orbits in their standard form, rather than the form in which

Table 5. Standard orbital elements and derived properties for HD 284163.

Property	Value
Inner orbit	
$P_{\rm A}$ (d)	2.39436657 ± 0.00000025
$T_{\rm peri,A}$ (HJD)	2454542.5452 ± 0.0077
$a''_{\rm A}$ (mas)	1.0071 ± 0.0044
$e_{\rm A}$	0.0557 ± 0.0011
$i_{\rm A}$ (deg)	72.93 ± 0.31
$\omega_{\rm Ab}$ (deg)	112.9 ± 1.2
$\Omega_{\rm A}$ (deg)	235.83 ± 0.29
$K_{\rm Aa}$ (km s^{-1})	66.786 ± 0.073
$K_{\rm Ab}$ (km s^{-1})	99.88 ± 0.55
Outer orbit	
$P_{\rm AB}$ (yr)	43.13 ± 0.10
$T_{\rm peri,AB}$ (yr)	1993.16 ± 0.13
$a''_{\rm AB}$ (arcsec)	0.3998 ± 0.0086
$e_{\rm AB}$	0.9154 ± 0.0039
$i_{\rm AB}$ (deg)	76.55 ± 0.31
$\omega_{\rm B}$ (deg)	78.01 ± 0.34
$\Omega_{\rm AB}$ (deg)	335.39 ± 0.46
$K_{\rm A}$ (km s^{-1})	7.8 ± 2.1
$K_{\rm B}$ (km s^{-1})	17.63 ± 0.81
γ (km s^{-1})	+37.620 ± 0.046
Derived properties	
$a_{\rm A}$ (R$_\odot$)	8.239 ± 0.032
$a_{\rm AB}$ (au)	15.21 ± 0.32
$M_{\rm Aa}$ (M$_\odot$)	0.784 ± 0.011
$M_{\rm Ab}$ (M$_\odot$)	0.5245 ± 0.0047
$q_{\rm A} \equiv M_{\rm Ab}/M_{\rm Aa}$	0.6686 ± 0.0036
$M_{\rm A}$ (M$_\odot$)	1.309 ± 0.015
$M_{\rm B}$ (M$_\odot$)	0.59 ± 0.12
$q_{\rm AB} \equiv M_{\rm B}/M_{\rm A}$	0.448 ± 0.089
$\pi_{\rm orb}$ (mas)	26.28 ± 0.16
Distance (pc)	38.05 ± 0.24
$i_{\rm rel}$ (deg)	94.94 ± 0.53

Note. Values represent the mode of the corresponding posterior distributions, which for the derived properties and some of the standard elements are constructed from those of the quantities involved from Table A1 in the Appendix.

[8] https://emcee.readthedocs.io/en/stable/index.html

some of them were used in the interest of numerical efficiency (see above). Full results for the 32 adjustable parameters, including the adopted priors, are given in the Appendix. The correlations among the elements of the inner and outer orbits from our analysis are shown graphically also in the Appendix.

The inner astrometric orbit is shown in Fig. 2, together with the CHARA observations. The corresponding outer orbit was shown previously in Section 2.3 (Fig. 1). An earlier astrometric solution for the outer orbit by Mason & Hartkopf (2010), based on fewer measurements, has a slightly smaller semimajor axis, and the position angle of the ascending node in the opposite quadrant because of the 180° ambiguity in some of the early speckle measurements. That ambiguity is resolved in modern speckle observations. A more recent orbit by Tokovinin (2023) is much closer to ours, with all of his elements being consistent with ours within their larger uncertainties.

Properties of the system derived from the orbital elements, such as the masses and orbital parallax, are given at the bottom of Table 5. Also included is the true inclination angle between the inner and outer orbital planes. Interestingly, the planes happen to be nearly perpendicular to each other ($i_{\rm rel} = 94.94 \pm 0.53$ degrees), formally representing retrograde motion. The eccentricity of the inner orbit is small, but clearly not zero. Tidal theory predicts that the orbit of stars like these with convective envelopes should be circularized on a time-scale of the order of 120 Myr (e.g. Hilditch 2001), which is significantly shorter than the age of the cluster (∼750 Myr; Brandt & Huang 2015). It is possible that the current eccentricity is being maintained by the presence of the tertiary in the system (see e.g. Mazeh 1990).

The orbital parallax we infer is $\pi_{\rm orb} = 26.28 \pm 0.16$ mas, compared to the value of 27.34 ± 0.39 mas in the *Gaia* DR3 catalogue (Gaia Collaboration 2023, source identifier 149767987810042624). However, the presence of the tertiary in HD 284163 appears to have degraded the quality of *Gaia*'s astrometric solution, as evidenced by a very large value of the renormalised unit weight error (RUWE).[9] *Gaia* sources with good-quality solutions have RUWE values typically smaller than 1.4, with a mean of 1.0, whereas HD 284163 has 22.4. This is not surprising, as the DR3 catalogue reports that the stellar profiles were double-peaked almost half of the time. This implies that the tertiary component was sometimes resolved, although the object was still analysed as single source. While this does not necessarily mean the *Gaia* parallax is incorrect, at the very least its uncertainty will be underestimated (see El-Badry, Rix & Heintz 2021). Following these authors, and correcting also for a zeropoint offset according to Lindegren et al. (2021), we arrive at a final adjusted *Gaia* parallax of 27.4 ± 1.1 mas, consistent with our much more precise value.

In Fig. 3, we display the radial velocities for the inner binary after subtracting the motion in the outer orbit. Fig. 4 shows the complementary plot of RVs in the outer orbit, with motion in the 2.39 d binary removed. The outer orbit is very eccentric ($e_{\rm AB} \approx 0.92$), and the spectroscopic observations unfortunately miss the periastron passage of 1993, which would have more strongly constrained the velocity amplitudes of the AB pair, strengthening the determination of the tertiary mass. Because the tertiary's orbit is so eccentric, the closest approach to the inner binary is only about 33 times the size of the inner orbit.

[9]For many of the multiple systems observed by *Gaia*, the processing for the DR3 catalogue included the derivation of astrometric or spectroscopic orbital solutions that generally improved the precision and accuracy of the astrometric results. Unfortunately, HD 284163 was not one of those systems with a derived orbit, likely because of the complicated nature of the source.

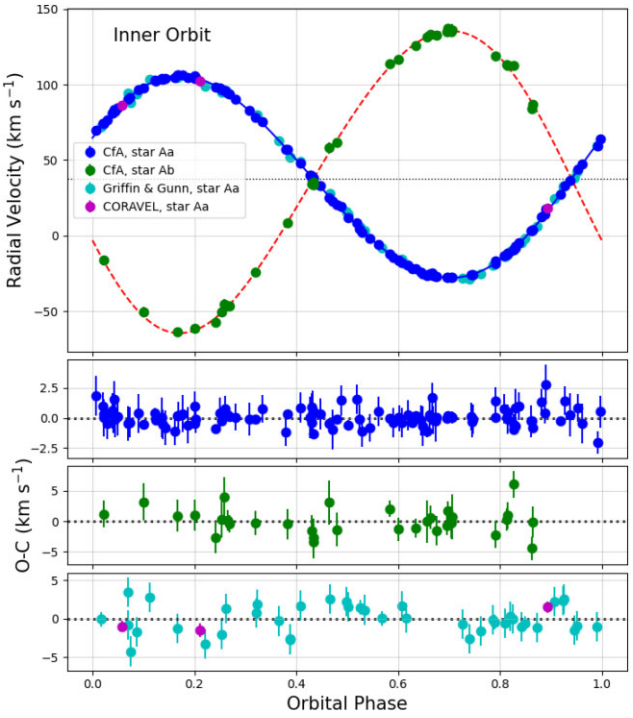

Figure 3. Radial-velocity measurements for HD 284163 in the inner orbit, as labelled, with motion in the outer orbit subtracted out. The dotted line marks the centre of mass velocity of the triple system. Residuals are shown at the bottom, separately for the CfA measurements of stars Aa and Ab, and other measurements of the primary.

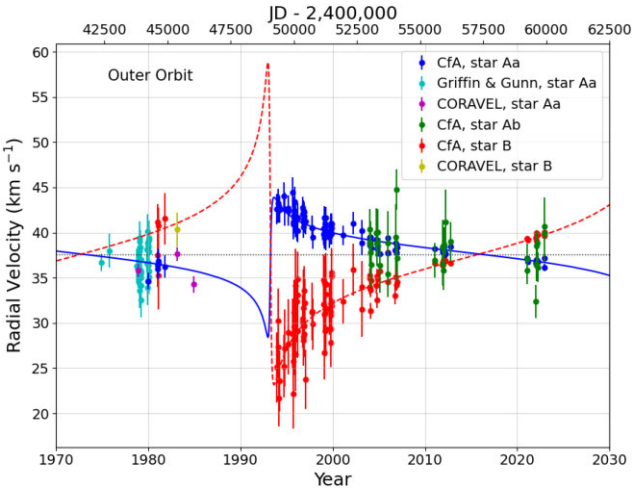

Figure 4. Radial-velocity measurements for HD 284163 in the outer orbit, after removing the motion in the inner orbit. The same colour scheme is used as in Fig. 3. The dotted line marks the centre-of-mass velocity of the triple system.

4 A FOURTH STAR IN THE HD 284163 SYSTEM

The WDS catalogue contains several measurements of a faint star some 5 arcsec south of HD 284163 AB, which has a separate entry in the *Gaia* DR3 catalogue (source identifier 149767987808179968). The proper motion and parallax listed by *Gaia* for this object are similar to those of the AB pair, suggesting physical association. The WDS measurements show a slight increase of ∼0.7 arcsec in the angular separation between 1997 and 2016, and about a 2°

change in the position angles over the same period, possibly due to orbital motion. This distant companion, which we refer to here as HD 284163 C, is about 4.3 mag fainter than the primary in the *Gaia* G band, but only about 1.3 mag fainter in K_S (Cutri et al. 2003), indicating it is a very red star.[10] Its radial velocity as reported by *Gaia* is 32.8 ± 5.1 km s^{-1}, with the large uncertainty most likely due to its faintness rather than intrinsic variability.

We have obtained two spectra of this star in 2004 using the CfA Digital Speedometer on the 1.5m telescope in Arizona, with signal-to-noise ratios of about 10 per resolution element. Cross-correlations against a range of templates observed with the same instrument indicate a best match against a spectrum of GJ 725 B, which is classified as M3.5 in the SIMBAD data base and M4.0 by Fouqué et al. (2018). Adopting a radial velocity of 1.19 ± 0.30 km s^{-1} for GJ 725 B from the latter source (in agreement with 1.18 ± 0.40 km s^{-1}, from Nidever et al. 2002), we obtain radial velocities for HD 284163 C of 36.61 ± 0.92 km s^{-1} on HJD 2453037.6904 and 36.39 ± 0.80 km s^{-1} on HJD 2453276.9417. The weighted average of these measurements, 36.48 ± 0.60 km s^{-1}, is only 1.1 ± 0.6 km s^{-1} lower than the centre-of-mass velocity γ of HD 284163 AB in Table 5, a difference consistent with being due to orbital motion.

All the evidence therefore points toward physical association with the brighter object, making HD 284163 a hierarchical quadruple system. At a distance to the Earth of 38 pc from Table 5, the projected linear separation of HD 284163 C is 190 au, from which we infer an orbital period of roughly 1700 yr.

5 STELLAR ACTIVITY

HD 284163 is classified as an RS CVn variable, and carries the designation V1136 Tau. In addition to the brightness changes motivating its classification, which are typically attributed to spots, it displays other classical signatures of chromospheric activity as documented by several authors beginning with Bopp, Africano & Goodrich (1986), and more recently also by Fang et al. (2018) and Ilin et al. (2021). The Ca II H and K lines, Hα, and the infrared Ca II triplet are all seen in emission. Fig. 5 shows this for the K line in our own TRES spectra, and demonstrates that all three components of the triple system are active. In particular, component Ab is fainter than component B, but seems to have stronger emission. We find that Hα is always in emission for the secondary, but not for the tertiary (which is a slow rotator; see Section 2.2), and only occasionally for the primary, though at a lower level. This is consistent with similar findings by Bopp, Africano & Goodrich (1986) (see footnote 1). The system is also an extreme ultraviolet source (McDonald et al. 1994), and an X-ray source, detected by both the *ROSAT* and *XMM–Newton* satellites.

Periodic brightness variations indicative of modulation by spots coming in and out of view have been observed, but not always. Bopp, Africano & Goodrich (1986) searched for variability in the early 1980s, but did not detect any significant variation. On the other hand, the recent *TESS* observations show it clearly (see Fig. 6). Rotation periods reported by various groups using different data sets consistently give values close to, but slightly shorter than the

[10]We note that the 2MASS catalogue indicates the near-infrared magnitudes of this companion may be biased by contamination from a nearby star, presumably the primary. In fact, the magnitudes of the primary star are also reported to be possibly contaminated by a diffraction spike from a nearby star, presumably the 5 arcsec companion.

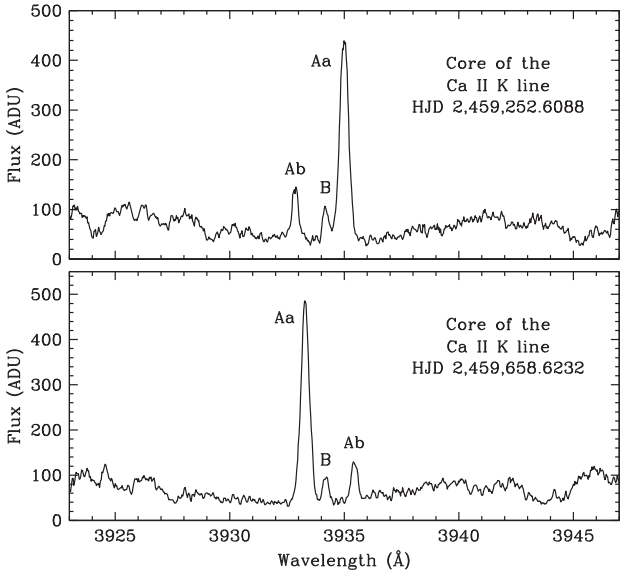

Figure 5. Central region of the Ca II K line in two of our TRES spectra, showing that all three components in HD 284163 exhibit emission cores, indicative of chromospheric activity. Components are labelled.

orbital period. Pojmanski (2002) obtained $P_{\rm rot} = 2.332$ d, with an amplitude of 0.07 mag in V, based on observations from the All-Sky Automated Survey. Photometry from the Hipparcos mission (source identifier HIP 19591) gave $P_{\rm rot} = 2.312$ d, and an amplitude of 0.09 mag (Rimoldini et al. 2012). Douglas et al. (2016) measured $P_{\rm rot} = 2.309$ d, and a total amplitude of 0.024 mag, using photometry from the Kepler/K2 mission. From Fig. 6, we obtained $P_{\rm rot} = 2.303 \pm 0.002$ d and a peak-to-peak amplitude of about 4 per cent in the *TESS* band. It is most likely that this period corresponds to the primary star, given that the secondary is much fainter, and that the tertiary is also fainter and much less active. All of these rotation period estimates are somewhat shorter than the pseudo-synchronous period (Hut 1981) for the primary, which is $P_{\rm pseudo} = 2.35$ d.

The photometric variability could explain some of the scatter we see in the CHARA flux ratios reported in Table 2. However, the differences in the table from epoch to epoch seem larger than can be expected from changes of just 5–10 per cent in the brightness of the primary, if we attribute the signal in Fig. 6 to that component alone. It seems likely, therefore, that the other components are variable as well, perhaps at a higher level than the primary percentage-wise, even though this may not be apparent in the light curve because of dilution from the brighter primary. Measurement errors may also contribute to the scatter.

6 DISCUSSION

Our dynamical mass determinations for the primary and secondary of HD 284163 are among the best in the Hyades (relative errors of 1.4 per cent and 0.9 per cent, respectively). The tertiary mass, on the other hand, is poorly determined mainly because of a lack of spectroscopic coverage of the outer orbit. The secondary is also the star with the lowest measured mass in the cluster to date, providing a useful extension of the empirical mass–luminosity relation toward the lower end.

This relation is shown in Fig. 7 for the visual band. Masses and absolute magnitudes for the seven binary and multiple systems in the Hyades reported prior to this work are taken from Torres, Stefanik &

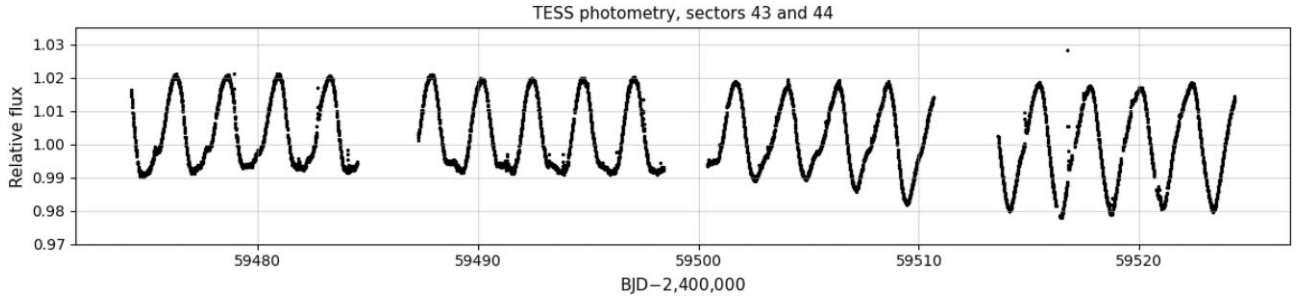

Figure 6. Photometry of HD 284163 from the *TESS* mission, as recorded in the full-frame images from sectors 43 and 44.[11] Gaps in the data occur during downlinks from the satellite. We attribute the variability to rotational modulation, and measure a rotation period of $P_{\rm rot} = 2.303 \pm 0.002$ d. Numerous flares are visible on closer inspection of the original data, the largest of which occurred on JD 2459516.75. It lasted for approximately 80 min, and boosted the overall brightness of HD 284163 by 4 per cent.

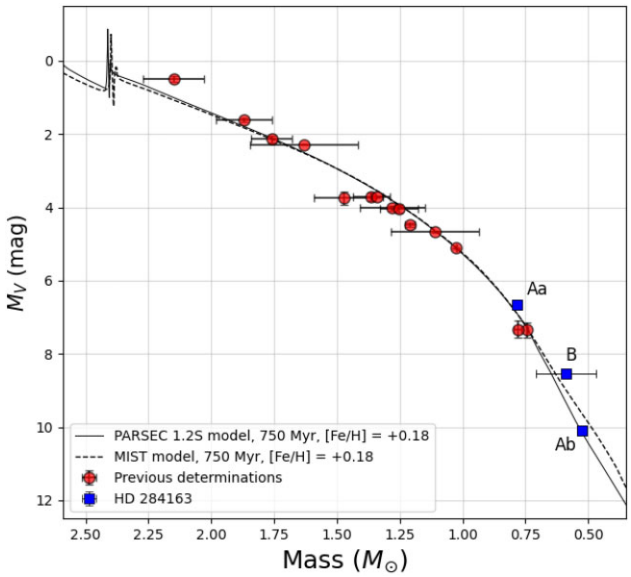

Figure 7. Empirical mass–luminosity relation in the Hyades, for the visual band. The observations are compared against two different model isochrones, as labelled, for the age and metallicity indicated (Brandt & Huang 2015; Dutra-Ferreira et al. 2016, respectively).

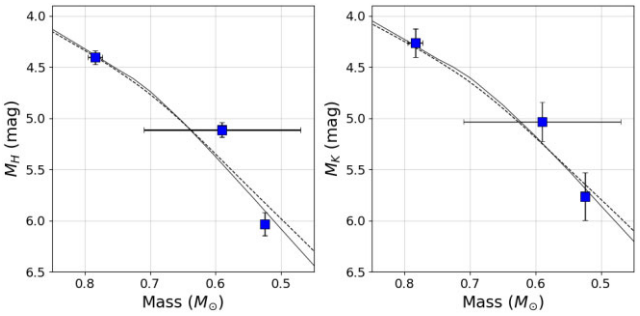

Figure 8. *H*- and *K*-band measurements for HD 284163 shown against the same models as in Fig. 7.

Latham (2019) and references therein, with updates for two of them (Brogaard et al. 2021; Anguita-Aguero et al. 2022). A complication for HD 284163 is that the overall brightness is somewhat uncertain because of the intrinsic variability. Reported *V*-band magnitudes differ by up to about 0.1 mag, ranging from $V = 9.342 \pm 0.004$ (Bopp, Africano & Goodrich 1986) to $V = 9.445 \pm 0.028$ (from the Tycho-2 magnitudes converted to the Johnson system; Høg et al. 2000). Changes in the average brightness were already noticed by Bopp, Africano & Goodrich (1986), who speculated that they could be related to long-term activity cycles in HD 284163, which are seen in other RS CVn systems. Here, we have chosen to adopt the brightest magnitude, on the assumption that all fainter values are impacted by spots. To deconvolve the combined light of the three stars, we used our spectroscopic flux ratios from Section 2.2, transformed to the *V* band. We did this with the aid of synthetic spectra appropriate for each star based on PHOENIX models by Husser et al. (2013), and interpolating the flux ratios between the Mg I b order and the *H* band. We obtained $f_{\rm Ab}/f_{\rm Aa}(V) = 0.043 \pm 0.004$ and $f_{\rm B}/f_{\rm Aa}(V) = 0.179 \pm 0.010$. HD 284163 was then placed on Fig. 7 using our orbital parallax from Table 5, and ignoring extinction.

Two model isochrones are shown in the figure, one from the PARSEC v1.2S series of Chen et al. (2014), and the other from the MIST series (Choi et al. 2016). The cluster age of 750 Myr and metallicity [Fe/H] = +0.18 adopted for this comparison are those proposed by Brandt & Huang (2015) and Dutra-Ferreira et al. (2016), respectively. The models generally fit the observations well, although formally the primary of HD 284163 is somewhat brighter than predicted. The most important difference between these series of models is in the lower main sequence, where the PARSEC v1.2S models have been tuned by the theorists to better match the observations of low-mass stars, by artificially altering the temperature–opacity relation below masses of about 0.75 $M_\odot$. This change is seen to work well for the secondary of HD 284163, whereas the standard MIST isochrone overpredicts its brightness.

The models fare better when compared against the absolute magnitudes in the near infrared. We computed these using the average of the *H*-band flux ratios in Table 2, and the single values available in *K*. For the latter, we adopted uncertainties equal to the standard deviation of the measurements in *H*. The adopted near-infrared flux ratios are $f_{\rm Ab}/f_{\rm Aa}(H) = 0.225 \pm 0.024$, $f_{\rm B}/f_{\rm Aa}(H) = 0.524 \pm 0.057$, $f_{\rm Ab}/f_{\rm Aa}(K) = 0.258 \pm 0.053$, and $f_{\rm B}/f_{\rm Aa}(H) = 0.51 \pm 0.13$. Fig. 8 shows the comparison for HD 284163. While both models agree in the *K* band with the measurements for the primary and secondary, in the *H* band only the PARSEC model fits the secondary within its error bar. None of the systems with previously published mass determinations can be shown in these diagrams, as the flux ratios and therefore the individual magnitudes are not known in the near infrared.

As a consistency check, we used our flux ratios in *V*, *H*, and *K* to compute the magnitude difference between the tertiary and the combined light of the inner binary, for comparison with independent

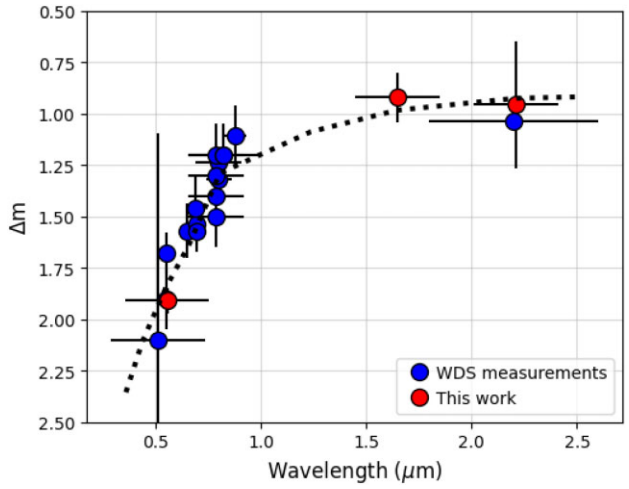

Figure 9. Magnitude difference between the tertiary (star B) and the combined light of the inner binary (Aa + Ab) of HD 284163, plotted as a function of wavelength. The horizontal error bars represent the width of each bandpass. The Δm estimates from our own spectroscopic and interferometric observations agree well with the trend from other determinations in the WDS, for which we adopted uncertainties of 10 per cent when not reported. The dotted line indicates the predicted wavelength dependence of Δm from the PARSEC v1.2S models of Chen et al. (2014). This is based on our measured masses for the primary and secondary, and a slightly adjusted mass for the tertiary, which is the most uncertain of the three. We find a good match between the model and the observations for a tertiary mass of 0.64 $M_\odot$, which is well within the formal uncertainty of the measured value (M_B = 0.59 ± 0.12 $M_\odot$; Table 5).

measurements at different wavelengths as listed in the WDS. This is shown in Fig. 9. Our measurements agree with the run of other empirical determinations, and follow the general trend predicted by stellar evolution models.

Finally, it is of interest to note that our orbital parallax places HD 284163 considerably closer to us (38 pc) than the cluster centre (47.5 pc; Gaia Collaboration 2018). This makes a difference of about 0.5 mag in the apparent brightness. The linear distance of HD 284163 from the centre of the cluster is about 11.2 pc. This is slightly outside of the ∼9 pc tidal radius of the Hyades (e.g. Röser et al. 2011; Jerabkova et al. 2021), where stars become more strongly influenced by the Galactic potential.

7 CONCLUSIONS

Our CHARA observations have allowed us to spatially resolve the inner 2.39 d binary in HD 284163, a very active RS CVn member of the Hyades cluster. The semimajor axis we measure is only 1 mas. A third component in the system, previously known from speckle observations, was also detected and has an updated orbital period of 43.1 yr. When combined with our RV measurements for the three stars, and others from the literature, we have established the 3D orbits of the components, and measured their dynamical masses, along with the orbital parallax. The inner and outer orbital planes are nearly at right angles to each other. The masses for the inner pair are good to better than 1.4 per cent, which are among the most precise in the cluster. Our observations have also provided measures of the relative brightness of the components, at optical as well as near-infrared wavelengths. A fourth, fainter component about 5 arcsec south is also known, and evidence is presented here that suggests it is physically associated, making HD 284163 a quadruple system.

This is the eighth multiple system in the Hyades with mass determinations. Comparison of the masses and absolute magnitudes with current stellar evolution models indicates a somewhat better fit in the near-infrared than in the optical, and that the PARSEC v1.2S models of Chen et al. (2014) match the observations of the low-mass secondary better than the standard MIST models (Choi et al. 2016).

ACKNOWLEDGEMENTS

The spectroscopic observations of HD 284163 at the CfA were obtained with the assistance of P. Berlind, M. Calkins, J. Caruso, G. Esquerdo, E. Horine, J. Peters, and J. Zajac. We thank them all. We also thank R. J. Davis and J. Mink for maintaining the data bases of echelle spectra, and the anonymous referee for helpful comments. This work is based upon observations obtained with the Georgia State University Center for High Angular Resolution Astronomy Array at Mount Wilson Observatory. The CHARA array was supported by the National Science Foundation under grant no. AST-1636624 and AST-2034336. Institutional support has been provided from the GSU College of Arts and Sciences and the GSU Office of the Vice President for Research and Economic Development. MIRC-X received funding from the European Research Council (ERC) under the European Union's Horizon 2020 research and innovation program (grant no. 639889). We thank J.-B. Le Bouquin for contributions to the MIRC-X/MYSTIC hardware and pipeline. JDM acknowledges funding for the development of MIRC-X (NASA-XRP NNX16AD43G, NSF-AST 1909165) and MYSTIC (NSF-ATI 1506540, NSF-AST 1909165). Time at the CHARA array was granted through the NOIRLab community access program (NOIRLab PropID: 2020B-0010, 2021B-0008, 2022B-235883; PI: G. Torres). This research has made use of the Jean-Marie Mariotti Center Aspro and SearchCal services. SK acknowledges support by the European Research Council (ERC Starting grant, no. 639889 and ERC Consolidator grant, no. 101003096), and STFC Consolidated Grant (ST/V000721/1). AL received funding from STFC studentship no. 630008203.

The research has made use of the SIMBAD and VizieR data bases, operated at the CDS, Strasbourg, France, of NASA's Astrophysics Data System Abstract Service, and of the Washington Double Star Catalog maintained at the U.S. Naval Observatory. We also used the WEBDA data base operated at the Department of Theoretical Physics and Astrophysics of the Masaryk University (Czech Republic).

The work has additionally made use of data from the European Space Agency (ESA) mission *Gaia* (https://www.cosmos.esa.int/gaia), processed by the *Gaia* Data Processing and Analysis Consortium (DPAC, https://www.cosmos.esa.int/web/gaia/dpac/consortium). Funding for the DPAC was provided by national institutions, in particular the institutions participating in the *Gaia* Multilateral Agreement. The computational resources used for this research include the Smithsonian High Performance Cluster (SI/HPC), Smithsonian Institution (https://doi.org/10.25572/SIHPC).

DATA AVAILABILITY

The data underlying this article are available in the article and in its online supplementary material.

REFERENCES

Anguita-Aguero J., Mendez R. A., Clavería R. M., Costa E., 2022, AJ, 163, 118

Anugu N. et al., 2020, Proc. SPIE Conf. Ser. Vol. 11446, Optical and Infrared Interferometry and Imaging VII. SPIE, Bellingham, p. 1144622

Anugu N. et al., 2020, AJ, 160, 158
Asensio-Torres R. et al., 2018, A&A, 619, A43
Bender C. F., Simon M., 2008, ApJ, 689, 416
Bopp B. W., Africano J. L., Goodrich B. D., 1986, PASP, 98, 457
Bourges L., Mella G., Lafrasse S., Duvert G., Chelli A., Le Bouquin J. -B., Delfossie X., Chesneau O., 2017, VizieR Online Data Catalog. p. II/346
Brandner W., Calissendorff P., Kopytova T., 2023, MNRAS, 518, 662
Brandt T. D., Huang C. X., 2015, ApJ, 807, 58
Brogaard K. et al., 2021, A&A, 645, A25
Che X. et al., 2013, J. Astron. Instrum., 2, 1340007
Chen Y., Girardi L., Bressan A., Marigo P., Barbeiri M., Kong X., 2014, MNRAS, 444, 2525
Choi J., Dotter A., Conroy C., Canteillo M., Paxton B., Johnson B. D., 2016, ApJ, 823, 102
Cutri R. M. et al., 2003, The IRSA 2MASS All-Sky Point Source Catalog, NASA/IPAC Infrared Science Archive. Available at: http://irsa.ipac.caltech.edu/applications/Gator/
Douglas S. T., Agüeros M. A., Covey K. R., Cargile P. A., Barclay T., Cody A., Howell S. B., Copytova T., 2016, ApJ, 822, 47
Dutra-Ferreira L., Pasquini L., Smiljanic R., Porto de Mello G. F., Steffen M., 2016, A&A, 585, A75
El-Badry K., Rix H. W., Heintz T. M., 2021, MNRAS, 506, 2269
Fang X.-S., Zhao G., Zhao J.-K., Bharat Kumar Y., 2018, MNRAS, 476, 908
Foreman-Mackey D., Hogg D. W., Lang D., Goodman J., 2013, PASP, 125, 306
Fouqué P. et al., 2018, MNRAS, 475, 1960
Fűrész G., 2008, PhD thesis, Univ. Szeged, Hungary
Gaia Collaboration, Brown A. G. A., Vallenari A. et al., 2018, A&A, 616, A1
Gaia Collaboration, Vallenari A., Brown A. G. A. et al., 2023, A&A, 674, A1
Gelman A., Rubin D. B., 1992, Stat. Sci., 7, 457
Griffin R. F., 2012, JA&A, 33, 29
Griffin R. F., Gunn J. E., 1981, AJ, 86, 588
Griffin R. F., Griffin R. E., Gunn J. E., Zimmerman B. A., 1985, AJ, 90, 609
Griffin R. F., Gunn J. E., Zimmerman B. A., Griffin R. E. M., 1988, AJ, 96, 172
Hilditch R. W., 2001, An Introduction to Close Binary Stars. Cambridge Univ. Press, Cambridge, UK, p. 152
Husser T. O., Wende-von Berg S., Dreizler S., Homeier D., Reiners A., Barman T., Hauschildt P. H., 2013, A&A, 553, A6
Hut P., 1981, A&A, 99, 126
Høg E. et al., 2000, A&A, 355, L27
Ilin E., Schmidt S. J., Poppenhäger K., Davenport J. R. A., Kristiansen M. H., Omohundro M., 2021, A&A, 645, A42
Irwin J. B., 1952, ApJ, 116, 211
Irwin J. B., 1959, AJ, 64, 149
Jerabkova T., Boffin H. M. J., Beccari G., de Marchi G., de Bruijne J. H. J., Prusti T., 2021, A&A, 647, A137
Latham D. W., 1992, in McAlister H. A., Hartkopf W. I., eds, ASP Conf. Ser. Vol. 32, Complementary Approaches to Double and Multiple Star Research, IAU Coll. 135, Astron. Soc. Pac., San Francisco, p. 110
Latham D. W., Stefanik R. P., Torres G., Davis R. J., Mazeh T., Carney B. W., Laird J. B., Morse J. A., 2002, AJ, 124, 1144
Lindegren L. et al., 2021, A&A, 649, A4
Luyten W. J., 1971, The Hyades, Monograph. Univ. of Minnesota, Minneapolis
McAlister H. A., Hartkopf W. I., Hutter D. J., 1987, AJ, 93, 688
McDonald K., Craig N., Sirk M. M., Drake J. J., Fruscione A., Vallerga J. V., Malina R. F., 1994, AJ, 108, 1843
Markwardt C. B., 2009, in Bohlender D. A., Durand D., Dowler P., eds, ASP Conf. Ser., Vol. 411, Astronomical Data Analysis Software and Systems XVIII. Astron. Soc. Pac., San Francisco, CA, p. 251
Mason B. D., Hartkopf W. I., 2010, IAU Inf. Circ., 170, 2
Mason B. D., Wycoff G. L., Hartkopf W. I., Douglass G. G., Worley C. E., 2001, AJ, 122, 3466
Mazeh T., 1990, AJ, 99, 675
Mermilliod J.-C., Mayor M., Udry S., 2009, A&A, 498, 949
Morzinski K. M., 2011, Ph.D. thesis, Univ. of California, Santa Cruz
Muirhead P. S., Nordhaus J., Drout M. R., 2022, AJ, 163, 34
Nidever D. L., Marcy G. W., Butler R. P., Fischer D. A., Vogt S. S., 2002, ApJS, 141, 503
Nordström B., Latham D. W., Morse J. A., Milone A. A. E., Curucz R. L., Andersen J., Stefanik R. P., 1994, A&A, 287, 338
Pels G., Oort J. H., Pels-Kluyver H. A., 1975, A&A, 43, 423
Pojmanski G., 2002, Acta Astron., 52, 397
Rimoldini L. et al., 2012, MNRAS, 427, 2917
Röser S., Schilbach E., Piskunov A. E. Kharchenko N. V. Scholz R.-D. 2011, A&A, 531, A92
Schaefer G. H., Hummel C. A., Gies D. R., 2016, AJ, 152, 213
Setterholm B. R. et al., 2023, J. Astron. Telesc. Instrum. Syst., 9, 025006
Stefanik R. P., Latham D. W., Torres G., 1999, in Hearnshaw J. B., Scarfe C. D., eds, ASP Conf. Ser. 185, Precise Stellar Radial Velocities, IAU Coll. 170. Astron. Soc. Pac., San Francisco, CA, p. 354
Szentgyorgyi A. H., Fűrész G., 2007, Rev. Mex. Astron. Astrofis, 28, 129
ten Brummelaar T. A. et al., 2005, ApJ, 628, 453
ten Brummelaar T. A. et al., 2016, in Malbet F., Creech-Eakman M. J., Tuthill P. G., eds, Proc. SPIE Conf. Ser. Vol. 9907, Optical and Infrared Interferometry and Imaging V. SPIE, Bellingham, p. 990703
Tokovinin A., 2023, IAU Inf. Circ., 209, 3
Tokovinin A., Thomas S., Sterzik M., Udry S., 2006, A&A, 450, 681
Toonen S., Hamers A., Portegies Zwart S., 2016, Comput. Astrophys. Cosmol., 3, 6
Torres G., Neuhäuser R., Guenther E. W., 2002, AJ, 123, 1701
Torres G., Andersen J., Giménez A., 2010, A&AR, 18, 67
Torres G., Stefanik R. P., Latham D. W., 2019, ApJ, 885, 9
Upgren A. R., Weis E. W., 1977, AJ, 82, 978
Worley C. E., Douglass G. G., 1997, A&AS, 125, 523
Zucker S., Mazeh T., 1994, ApJ, 420, 806
Zucker S., Torres G., Mazeh T., 1995, ApJ, 452, 863

SUPPORTING INFORMATION

Supplementary data are available at *MNRAS* online.

Table 4. CfA radial velocity measurements for HD 284163.

Please note: Oxford University Press is not responsible for the content or functionality of any supporting materials supplied by the authors. Any queries (other than missing material) should be directed to the corresponding author for the article.

APPENDIX

This appendix provides the details of our MCMC analysis. Table A1 gives the results for the 32 free parameters, listed in the form in which they were adjusted (see the main text in Section 3).

Figs A1 and A2 show the correlations among the elements of the inner and outer orbits of HD 284163, respectively, based on the posterior distributions from our MCMC analysis. The elements of the outer orbit display higher correlations, as expected from the more incomplete observational coverage.

Table A1. Full set of adjusted parameters for HD 284163.

Parameter	Value	Prior
	Inner orbit	
$P_{\rm A}$ (d)	2.39436657 ± 0.00000025	[2, 3]
$T_{\rm peri,A}$ (HJD)[a]	54542.5452 ± 0.0077	[54541, 54543]
$a''_{\rm A}$ (mas)	1.0071 ± 0.0044	[0.5, 2.0]
$\sqrt{e_{\rm A}}\cos\omega_{\rm Ab}$	−0.0918 ± 0.0043	[−1, 1]
$\sqrt{e_{\rm A}}\sin\omega_{\rm Ab}$	+0.2174 ± 0.0031	[−1, 1]
$\cos i_{\rm A}$	0.2936 ± 0.0052	[−1, 1]
$\Omega_{\rm A}$ (deg)	235.83 ± 0.29	[0, 360]
$K_{\rm Aa}$ (km s^{-1})	66.786 ± 0.073	[50, 150]
$K_{\rm Ab}$ (km s^{-1})	99.88 ± 0.55	[50, 150]
	Outer orbit	
$P_{\rm AB}$ (yr)	43.13 ± 0.10	[30, 50]
$T_{\rm peri,AB}$ (yr)	1993.16 ± 0.13	[1980, 2010]
$a''_{\rm AB}$ ($''$)	0.3998 ± 0.0086	[0.1, 0.6]
$\sqrt{e_{\rm AB}}\cos\omega_{\rm B}$	+0.1987 ± 0.0051	[−1, 1]
$\sqrt{e_{\rm AB}}\sin\omega_{\rm B}$	+0.9359 ± 0.0031	[−1, 1]
$\cos i_{\rm AB}$	0.2325 ± 0.0053	[−1, 1]
$\Omega_{\rm AB}$ (deg)	335.39 ± 0.46	[0, 360]
$K_{\rm B}$ (km s^{-1})	17.63 ± 0.81	[0, 50]
	Other spectroscopic parameters	
γ (km s^{-1})	+37.620 ± 0.046	[20, 50]
$\Delta_{\rm DS}$ (km s^{-1})	−0.32 ± 0.73	[−10, 10]
$\Delta_{\rm TRES}$ (km s^{-1})	+1.35 ± 0.52	[−10, 10]
$\Delta_{\rm GG}$ (km s^{-1})	+0.10 ± 0.27	[−10, 10]
	Astrometric error inflation factors	
f_θ	2.24 ± 0.41	[−5, 5]
f_ρ	2.69 ± 0.53	[−5, 5]
$f_{\rm CHARA,A}$	1.44 ± 0.50	[−5, 5]
$f_{\rm CHARA,AB}$	5.8 ± 2.2	[−5, 5]
	Spectroscopic error inflation factors	
$f_{\rm Aa,DS}$	0.914 ± 0.080	[−5, 5]
$f_{\rm Ab,DS}$	1.32 ± 0.34	[−5, 5]
$f_{\rm B,DS}$	1.062 ± 0.093	[−5, 5]
$f_{\rm Aa,TRES}$	1.32 ± 0.30	[−5, 5]
$f_{\rm Ab,TRES}$	0.99 ± 0.23	[−5, 5]
$f_{\rm B,TRES}$	1.05 ± 0.25	[−5, 5]
$f_{\rm Aa,GG}$	1.06 ± 0.14	[−5, 5]

Notes. Values listed correspond to the mode of the respective posterior distributions, with uncertainties representing the 68.3 per cent credible intervals. Priors in square brackets are uniform over the ranges specified, except those for the error inflation factors f, which are log-uniform.
[a]The time of periastron passage is referenced to HJD 2400000.

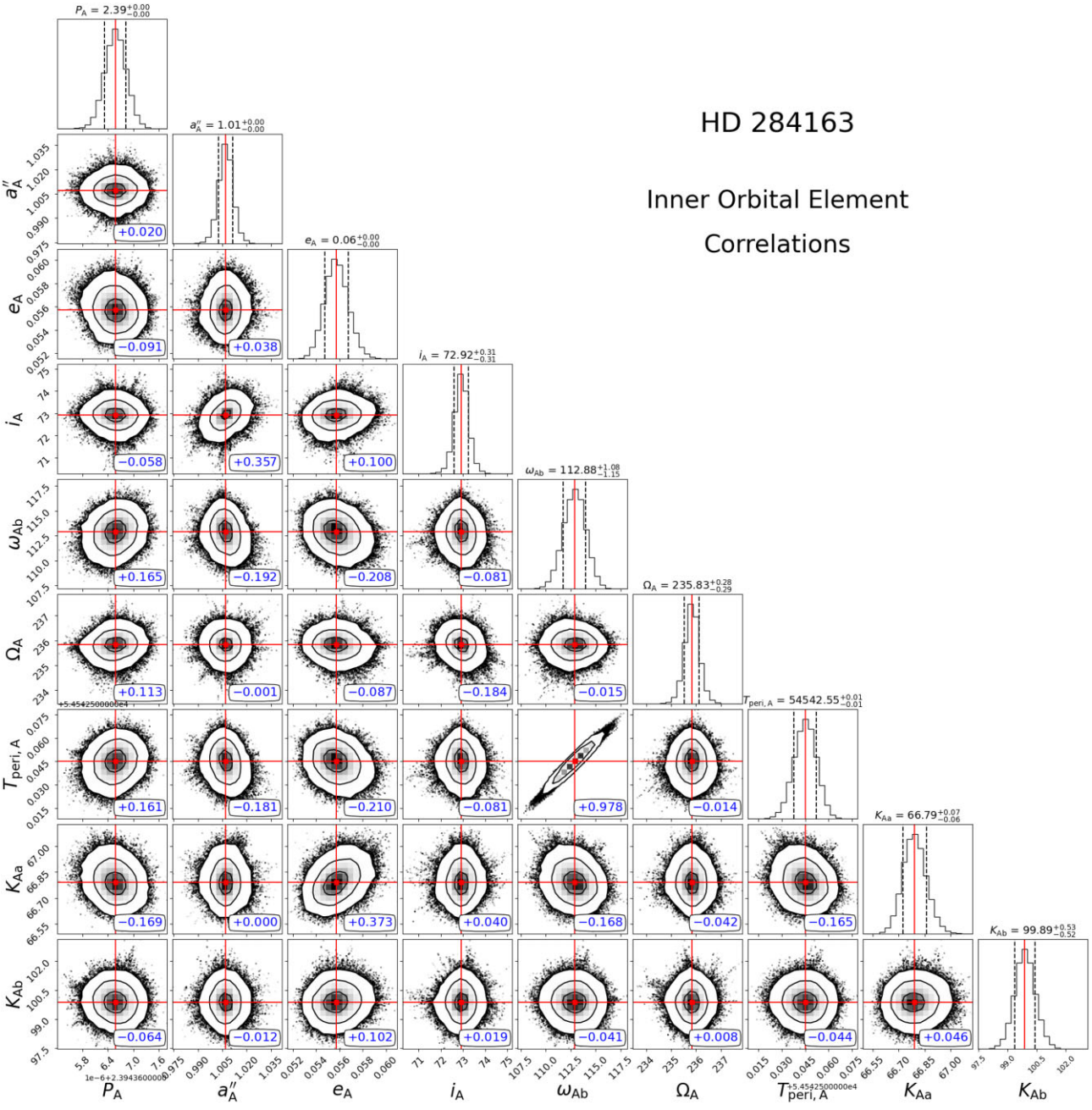

Figure A1. Correlations among the elements of the inner orbit of HD 284163. The contours represent the 1, 2, and 3σ confidence levels. The correlation coefficients are indicated in each panel.

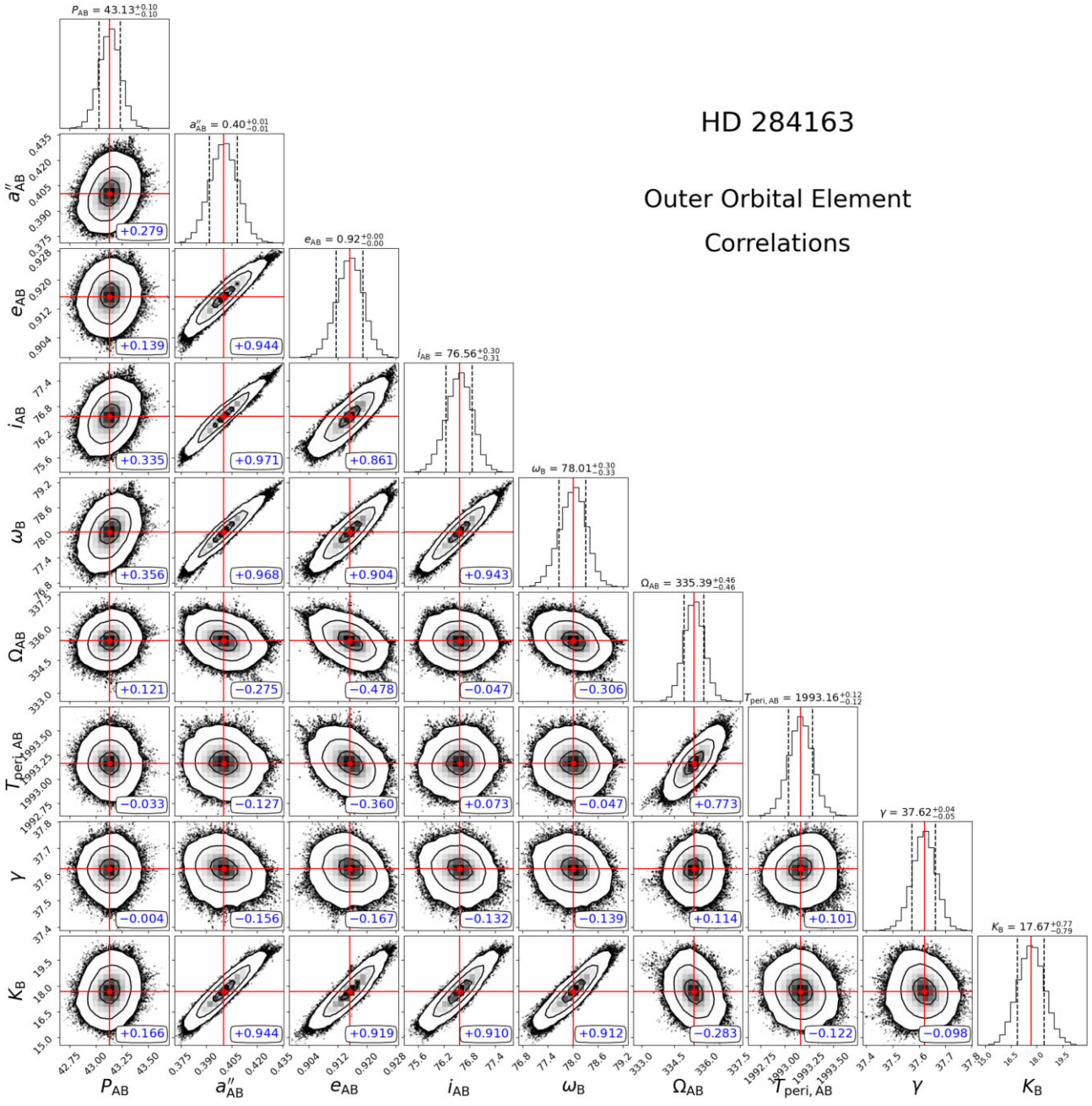

Figure A2. Correlations among the elements of the outer orbit of HD 284163. The contours represent the 1, 2, and 3σ confidence levels. The correlation coefficients are indicated in each panel.

This paper has been typeset from a TEX/LATEX file prepared by the author.